

# Exact treatment of exciton-polaron formation by Diagrammatic Monte Carlo

Evgeni Burovski,<sup>1,2</sup> Holger Fehske,<sup>2</sup> and Andrei S. Mishchenko<sup>3,4</sup>

<sup>1</sup>*Laboratoire de Physique Théorique et Modèles Statistiques, Université Paris-Sud, 91405 Orsay Cedex, France*

<sup>2</sup>*Institut für Physik, Ernst-Moritz-Arndt-Universität Greifswald, 17489 Greifswald, Germany*

<sup>3</sup>*Cross-Correlated Materials Research Group, RIKEN, 2-1 Hirosawa, Wako, Saitama, 351-0198, Japan*

<sup>4</sup>*Russian Research Centre "Kurchatov Institute", 123182 Moscow, Russia*

We develop an approximation-free Diagrammatic Monte Carlo technique to study fermionic particles interacting with each other simultaneously through both an attractive Coulomb potential and bosonic excitations of the underlying medium. Exemplarily we apply the method to the long-standing exciton-polaron problem and present numerically exact results for the wave function, ground-state energy, binding energy and effective mass of this quasiparticle. Focusing on the electron-hole pair bound-state formation, we discuss various limiting cases of a generic exciton-polaron model. The frequently used instantaneous approximation to the retarded interaction due to the phonon exchange is found to be of very limited applicability. For the case of a light electron and heavy hole the system is well approximated by a particle in the field of a static attractive impurity.

PACS numbers: 71.35.-y, 02.70.Ss, 71.38.-k

The problem of two quasiparticles (QPs) interacting via instantaneous Coulomb interaction and a retarded exchange of bosons is a tremendously difficult stumbling block in solid state many-particle physics [1, 2, 3]. The variety of such objects range from exciton-polarons (EX-P) in semiconductors, where (opposite) charged holes (H) and electrons (E) couple to lattice vibrations (phonons) [2], to more exotic situations e.g. in the context of high- $T_c$  superconductivity, where two holes may form a bound state in an antiferromagnetically correlated background due to exchange of spin excitations (magnons) [4].

First attempts to tackle the EX-P problem are restricted to low-dimensional cases, and reduce the two QPs to a preformed structureless QP object [3, 5]. Moreover the rather crude adiabatic approximation was frequently used [3], as well as simple variational approaches [6]. Quite recently a quantum Monte Carlo study has been carried out [7], but for a one-dimensional (1D) model with simplified Coulomb and E/H-phonon interactions. In any case, a general approximation-free method for treating a system of interacting QPs in bosonic fields is missing. Even the interaction of two QPs through an instantaneous potential creates enormous technical difficulties. For 3D situations with realistic QP dispersions, at the moment, Diagrammatic Monte Carlo (DMC) [8] and Bethe-Salpeter [9] methods seem to be the most promising techniques to address such problems. Within a Bethe-Salpeter based approach coupling to phonons can be introduced only in a less controllable phenomenological way [10] and we are not aware of any generalization to a true full-scale problem. By contrast, we will demonstrate that a corresponding generalization of the DMC method can be done in a rigorous way.

In the present paper we develop such a general approximation-free DMC technique and apply it for the first time to the highly non-trivial EX-P problem. Note

that different from direct-space DMC [11] our method is realized in momentum space and will thus not be restricted to the treatment of finite systems. Furthermore the proposed momentum space DMC approach is capable of describing dispersive fermions and bosons, as well as (long-range) interactions between those objects in any dimension. It is used to obtain the EX-P wave function, energy, and mass, also for the case when an E-H bound state arises due to cooperative effect of short-range Coulomb attraction and exchange of phonons. In addition we determine the ground-state phase diagram for a restricted EX-P model with contact Coulomb and particle-phonon interaction, discuss important limiting cases and the validity of approximative solutions.

To this end let us start from the following Hamiltonian

$$\begin{aligned}
 H = & \sum_{\mathbf{k}} \varepsilon_c(\mathbf{k}) e_{\mathbf{k}}^{\dagger} e_{\mathbf{k}} + \sum_{\mathbf{k}} \varepsilon_v(\mathbf{k}) h_{\mathbf{k}} h_{\mathbf{k}}^{\dagger} + \sum_{\mathbf{q}} \omega_{\mathbf{q}} b_{\mathbf{q}}^{\dagger} b_{\mathbf{q}} \\
 & - \sum_{\mathbf{k}\mathbf{q}} \left[ \frac{g_e(\mathbf{q})}{\sqrt{N}} e_{\mathbf{k}-\mathbf{q}}^{\dagger} e_{\mathbf{k}} + \frac{g_h(\mathbf{q})}{\sqrt{N}} h_{\mathbf{k}-\mathbf{q}}^{\dagger} h_{\mathbf{k}} \right] (b_{\mathbf{q}}^{\dagger} + b_{-\mathbf{q}}) \\
 & - \sum_{\mathbf{p}\mathbf{k}\mathbf{k}'} \frac{U(\mathbf{p}, \mathbf{k}, \mathbf{k}')}{N} e_{\mathbf{k}}^{\dagger} h_{\mathbf{p}-\mathbf{k}}^{\dagger} h_{\mathbf{p}-\mathbf{k}'} e_{\mathbf{k}'} . \quad (1)
 \end{aligned}$$

Here  $e_{\mathbf{k}}$  ( $h_{\mathbf{k}}$ ) annihilates an E (H) in the conduction (valence) band with dispersion  $\varepsilon_c(\mathbf{k})$  ( $\varepsilon_v(\mathbf{k})$ ) and  $b_{\mathbf{q}}$  is the corresponding annihilation operator for a phonon with momentum  $\mathbf{q}$ . In (1),  $U(\mathbf{p}, \mathbf{k}, \mathbf{k}')$  describes the attractive interband interaction and  $g_e(\mathbf{q})$  ( $g_h(\mathbf{q})$ ) the E(H)-phonon coupling.  $N$  denotes the number of lattice sites. We work in the thermodynamic limit  $N \rightarrow \infty$ .

An energy ( $E_{\nu}(\mathbf{p})$ ) momentum ( $\mathbf{p}$ ) eigenstate ( $|\nu; \mathbf{p}\rangle$ ) of  $H$  can be expressed as linear combination

$$|\nu; \mathbf{p}\rangle = \sum_{M=0}^{\infty} \sum_{\{\mathbf{q}\}\mathbf{k}} \xi_{\mathbf{p}\mathbf{k}}^{M\{\mathbf{q}\}}(\nu) Y_{\mathbf{p}\mathbf{k}}^{M\{\mathbf{q}\}\dagger} |\text{vac}\rangle \quad (2)$$

of E-H pair basis states in the presence of  $M$

phonons (having momenta  $\mathbf{q}_1, \dots, \mathbf{q}_M$ ), where  $Y_{\mathbf{p}\mathbf{k}}^{M\{\mathbf{q}\}} \equiv e_{\mathbf{k}} h_{\mathbf{p}-\mathbf{k}-\sum_{j=1}^M \mathbf{q}_j} \prod_{j=1}^M b_{\mathbf{q}_j}$ . The  $M = 0$  term is understood as  $Y_{\mathbf{p}\mathbf{k}}^{M=0} = e_{\mathbf{k}} h_{\mathbf{p}-\mathbf{k}}$ . Within this basis we define the two-particle imaginary-time Green function (GF) with center-of-mass momentum  $\mathbf{p}$  as

$$G_{\mathbf{p},\mathbf{k}}^{M\{\mathbf{q}\}}(\tau) = \langle \text{vac} | Y_{\mathbf{p}\mathbf{k}}^{M\{\mathbf{q}\}}(\tau) Y_{\mathbf{p}\mathbf{k}}^{M\{\mathbf{q}\}\dagger}(0) | \text{vac} \rangle, \quad (3)$$

where  $Y(\tau) = e^{H\tau} Y e^{-H\tau}$  ( $\tau > 0$ ), and  $|\text{vac}\rangle$  is a direct product of the phonon vacuum and completely filled (empty) valence (conduction) bands. Rewriting (3) in interaction representation and expanding it in terms of both Coulomb interaction  $U$  and E(H)-phonon couplings  $g_{e,h}$ , one arrives at a series of phonon-dressed ladder-type Feynman diagrams [12], cf. Fig. 1. The weight attributed to a given diagram is the product of the interaction vertices ( $U(\mathbf{p}, \mathbf{k}, \mathbf{k}')$ ,  $g_e(\mathbf{q})$ , and  $g_h(\mathbf{q})$ ) and Matsubara GFs of holes, electrons, and phonons with the corresponding imaginary times and momenta subjected to momentum conservation imposed by the Hamiltonian (1).

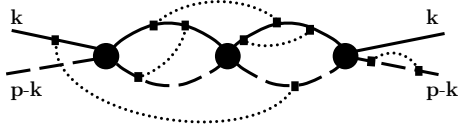


FIG. 1: A typical diagram for  $G_{\mathbf{p},\mathbf{k}}^{M=0}(\tau)$ . Solid (dashed) line represent E (H) propagators, solid circles (squares) designate Coulomb (QP-phonon) interactions, and dotted lines are the phonon propagators. Imaginary time runs from left to right.

In the numerical work, the Monte Carlo updates of diagonal phonon propagators (connecting two points  $\tau_1$  and  $\tau_2$  of the same QP propagator) were performed by the DMC technique developed for a polaron [13, 14], while Coulomb vertices are updated as for the pure exciton problem [8]. The new update for nondiagonal phonon propagators (see Fig. 2) requires special care to maintain the momentum conservation. When updating diagonal phonon contributions, momentum conservation is simply achieved by subtracting the phonon momentum from all QP propagators between  $\tau_1$  and  $\tau_2$  [13, 14]. Such strategy is not suitable for the non-diagonal phonon propagators since the phonon momentum is taken from one QP line and absorbed by another one. The problem can be solved, however, by absorbing the momentum transfer into the Coulomb vertex which, in circular representation for the GF [8, 14], always appears either to the left of the phonon propagator ( $\tau_a$  in Fig. 2a) or between  $\tau_1$  and  $\tau_2$  ( $\tau_b$  in Fig. 2a). As illustrated in Fig. 2b, in the first case the phonon momentum  $\mathbf{Q}$  is subtracted (added) to (from) the E (H) propagators located between the Coulomb vertex at  $\tau_a$  and  $\tau_1$  ( $\tau_2$ ). In the second case, the E (H) momenta are changed as  $\mathbf{k} \rightarrow \mathbf{k} - \mathbf{Q}$  for  $\tau' \in [\tau_b, \tau_2]$  ( $\tau' \in [\tau_1, \tau_b]$ ), see Fig. 2c. Note that at any  $\tau'$  the total

momentum of E, H, and phonons is equal to the center-of-mass momentum  $\mathbf{p}$ .

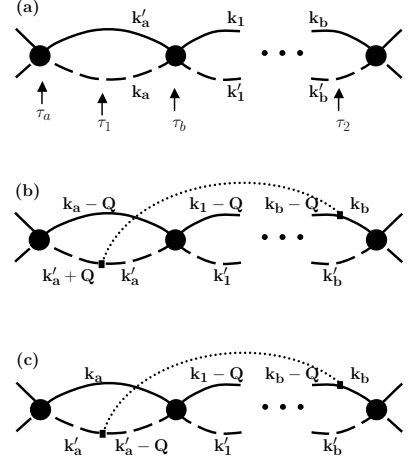


FIG. 2: The way how momentum conservation is ensured (b-c) when a nondiagonal phonon is added to configuration (a). Diagrams with a non-diagonal phonon line and no Coulomb vertices are prohibited by momentum conservation in (3).

Now the EX-P's energy, effective mass, and wave function can be found by DMC sampling of GFs at times larger than the reciprocal energy difference between the ground  $|\text{g.s.}\rangle$  and the first excited state,  $\tau > \tau_{\text{lim}}$ . Inserting the complete set (2) into (3), we have

$$G_{\mathbf{p},\mathbf{k}}^{M\{\mathbf{q}\}}(\tau) = \sum_{\nu} \left| \xi_{\mathbf{p}\mathbf{k}}^{M\{\mathbf{q}\}}(\nu) \right|^2 e^{-\tau E_{\nu}(\mathbf{p})}. \quad (4)$$

For  $\tau \geq \tau_{\text{lim}}$  the GF projects onto the ground state in the  $\mathbf{p}$ -sector [8, 13, 14]:

$$G_{\mathbf{p},\mathbf{k}}^{M\{\mathbf{q}\}}(\tau \rightarrow \infty) \rightarrow \left| \xi_{\mathbf{p}\mathbf{k}}^{M\{\mathbf{q}\}}(\text{g.s.}) \right|^2 e^{-\tau E_{\text{g.s.}}(\mathbf{p})}. \quad (5)$$

Due to the normalization  $\sum_{M=0}^{\infty} \sum_{\{\mathbf{q}\}\mathbf{k}} \left| \xi_{\mathbf{p}\mathbf{k}}^{M\{\mathbf{q}\}}(\nu) \right|^2 = 1$ , the sum of all possible  $M$ -phonon GFs [14],

$$\mathfrak{G}_{\mathbf{p}}(\tau) = \sum_{M=0}^{\infty} \sum_{\{\mathbf{q}\}\mathbf{k}} G_{\mathbf{p},\mathbf{k}}^{M\{\mathbf{q}\}}(\tau), \quad (6)$$

has an especially simple asymptotic form,  $\mathfrak{G}_{\mathbf{p}}(\tau \rightarrow \infty) \rightarrow e^{-\tau E_{\text{g.s.}}(\mathbf{p})}$ . According to (5) and (6) the estimators for the amplitudes  $\xi_{\mathbf{p}\mathbf{k}}^{M\{\mathbf{q}\}}(\text{g.s.})$  are related to the distribution of variables  $M$ ,  $\{\mathbf{q}\}$  and  $\mathbf{k}$  which are all generated by the DMC algorithm  $G_{\mathbf{p},\mathbf{k}}^{M\{\mathbf{q}\}}(\tau)/\mathfrak{G}_{\mathbf{p}}(\tau) |_{\tau \rightarrow \infty} \rightarrow \left| \xi_{\mathbf{p}\mathbf{k}}^{M\{\mathbf{q}\}}(\text{g.s.}) \right|^2$ . Since the whole set  $\{\xi_{\mathbf{p}\mathbf{k}}^{M\{\mathbf{q}\}}(\text{g.s.})\}$ , defining the inner structure of the EX-P state, is difficult to visualize, we introduce integrated quantities. For example, the integrated  $Z$ -factor  $Z_{\mathbf{p}}^{(M)} = \sum_{\mathbf{k}\{\mathbf{q}\}} \left| \xi_{\mathbf{p}\mathbf{k}}^{M\{\mathbf{q}\}}(\text{g.s.}) \right|^2$  measures the partial weights of  $M$ -phonon configurations

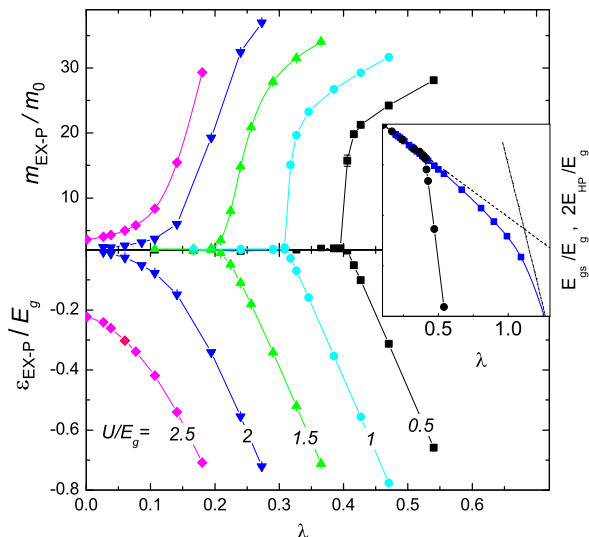


FIG. 3: (Color online) Binding energy  $\varepsilon_{\text{EX-P}}$  (in units of the gap  $E_g$ ) and effective mass  $m_{\text{EX-P}}$  (in units of  $m_0 = E_{c,v}/6$ ) as functions of E/H-phonon coupling  $\lambda$  for  $\Omega = 0.25E_g$ . The inset shows the EX-P energy  $E_{\text{g.s.}}$  (circles) compared to  $2E_{\text{HP}}$  (squares) at  $U/E_g = 1$ . Statistical error bars are smaller than symbol size. Dot-dashed lines indicate the HP strong- and weak-coupling results.

in the phonon cloud of an EX-P with center-of-mass momentum  $\mathbf{p}$ . On the other hand, for a given eigenstate  $|\nu; \mathbf{p}\rangle$  of (1), the probability  $W(\mathbf{P}, \mathbf{K})$  for a E-H pair to have center-of-mass momentum  $\mathbf{P}$  and relative momentum  $\mathbf{K}$  is obtained by tracing out the phonons from the density matrix  $\rho = |\nu; \mathbf{p}\rangle\langle\nu; \mathbf{p}|$ :

$$W(\mathbf{P}, \mathbf{K}) = \sum_{M=0}^{\infty} \sum_{\{\mathbf{q}_j\}} \left| \xi_{\mathbf{p}\mathbf{K}}^{M\{\mathbf{q}_j\}} \right|^2 \delta \left( \mathbf{p} - \sum_{j=1}^M \mathbf{q}_j - \mathbf{P} \right). \quad (7)$$

In order to validate this novel technique, we now investigate a minimal 3D simple-cubic (tight-binding) two-band model,  $\varepsilon_{c,v}(\mathbf{k}) = \tilde{E}_{c,v} \pm (E_{c,v}/6) \sum_{\alpha=x,y,z} (1 - \cos k_\alpha)$ , where  $\tilde{E}_c = E_g$  gives the direct gap at  $\mathbf{k} = 0$ ,  $\tilde{E}_v = 0$ , and  $E_c$  and  $E_v$  are the bandwidths of the conduction and valence bands, respectively. Furthermore, we take the phonon frequency  $\omega_{\mathbf{q}} \equiv \Omega$ , particle-phonon couplings  $g_{e,h}(\mathbf{q}) \equiv g$ , and the interband Coulomb attraction  $U(\mathbf{p}, \mathbf{k}, \mathbf{k}') \equiv U$  as momentum independent. A distinctive feature of this model is that E and H only form a bound state if  $U > U_*$ , where  $U_*^{-1} = N^{-1} \sum_{\mathbf{k} \in \text{BZ}} (\varepsilon_c(\mathbf{k}) - \varepsilon_v(\mathbf{k}) - E_g)^{-1}$ . Hence, depending on the Coulomb attraction  $U$  and the dimensionless E/H-phonon coupling  $\lambda = 2g^2/(\Omega E_c)$ , the EX-P binding energy  $\varepsilon_{\text{EX-P}} \equiv E_{\text{g.s.}} - 2E_{\text{HP}}$  (defined as the difference between the EX-P ground-state energy  $E_{\text{g.s.}}$  and twice the ground-state energy of a single electron/hole Holstein polaron (HP)  $E_{\text{HP}}$  at  $\mathbf{p} = 0$  [15]), is either  $\varepsilon_{\text{EX-P}} = 0$  (unbound state) or  $\varepsilon_{\text{EX-P}} < 0$  (bound state).

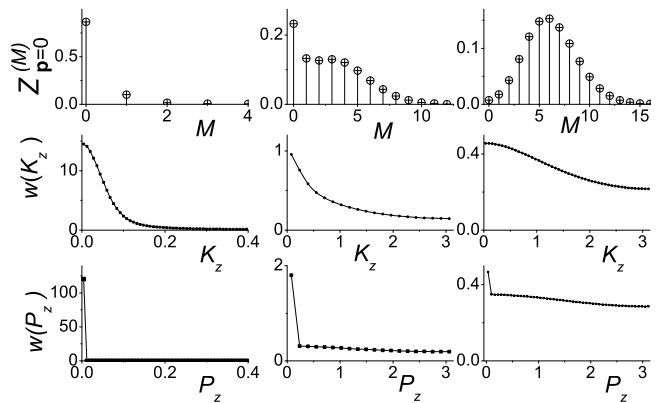


FIG. 4: Internal structure of an EX-P in the mass-symmetric model with  $U = 1.5E_g$  and  $\lambda = 0.195 < \lambda_*$  (1st column),  $\lambda = 0.223 \approx \lambda_*$  (2nd column),  $\lambda = 0.29 > \lambda_*$  (3rd column). First row shows the integrated Z-factors, second (third) row displays the reduced distributions of  $W(\mathbf{P}, \mathbf{K})$  (7)  $w(K_z) \equiv \int d^3 P dK_x dK_y W(\mathbf{P}, \mathbf{K})$  ( $w(P_z) \equiv \int d^3 K dP_x dP_y W(\mathbf{P}, \mathbf{K})$ ).

Figure 3 presents the data for the mass-symmetric model with  $E_c = E_v = 3E_g$  and  $\Omega = 0.25E_g$ . Here the critical Coulomb attraction is  $U_* \approx 1.98E_g$ , i.e. for  $U/E_g = 2.5$  the H and E are already bound at  $\lambda = 0$ . As  $\lambda$  is increased, the EX-P binding energy and effective mass smoothly increase and finally show the standard weak- to strong-coupling crossover [16]. By contrast, for  $U < U_*$ , a critical coupling  $\lambda_*(U)$  is required to create the EX-P bound state. While here the single HP exhibits a rather smooth crossover from a weakly to strongly mass-renormalized QP at about  $\lambda \approx 1$  (see inset in Fig. 3), the transition of the E-H pair from unbound to bound state is accompanied by a much more rapid change of EX-P properties (Fig. 3). The sharper crossover to the small radius EX-P regime can be understood from the increasing importance of the QP-phonon coupling when the EX-QP bound state is established [17]. In accordance with Ref. [11] we find  $\lambda_*(U = 0) \approx 0.5$ .

The internal structure of the  $\mathbf{p} = 0$  EX-P state significantly changes at the unbound-to-bound-state transition (Fig. 4). For  $\lambda < \lambda_*$  the E-H pair is only weakly dressed by phonons leading to  $\mathbf{P} \approx 0$ . The distribution of the relative momentum  $\mathbf{K}$  is narrow, pointing to a large real space separation of the E-H pair. For  $\lambda \geq \lambda_*$ , E and H are confined and the  $\mathbf{K}$  distribution broadens. At the same time the  $\mathbf{P}$  distribution develops a shoulder due to fluctuations of the momentum of the phonon cloud, and the amplitude of the peak at  $\mathbf{P} = 0$  decreases, reflecting the suppression of the zero-phonon weight. For  $\lambda > \lambda_*$  the phonon distribution  $Z^{(M)}$  is almost Gaussian [14]. In the  $\lambda \approx \lambda_*$  region, the  $Z^{(M)}$ -factor distribution shows a kind of “bimodality” which, however, is only observed provided that  $\Omega \ll E_{c,v}$ . This feature rapidly disappears for larger phonon frequencies [5].

For finite  $\Omega$ , the phonon exchange leads to a retarded

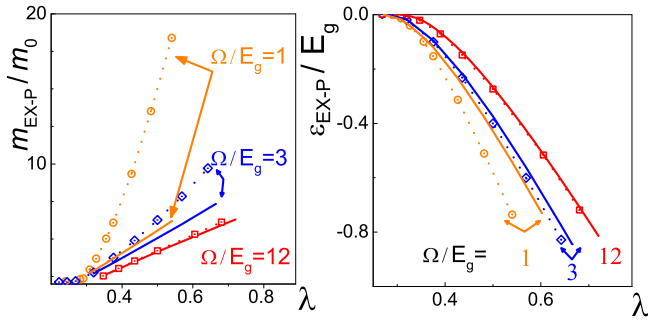


FIG. 5: (Color online) Exact DMC EX-P energy and effective mass (symbols with dotted lines, statistical errors are smaller than the symbol size) compared to results for the EAHM (solid lines). Data obtained for  $U = E_g$  and  $E_c = E_v = 3E_g$ .

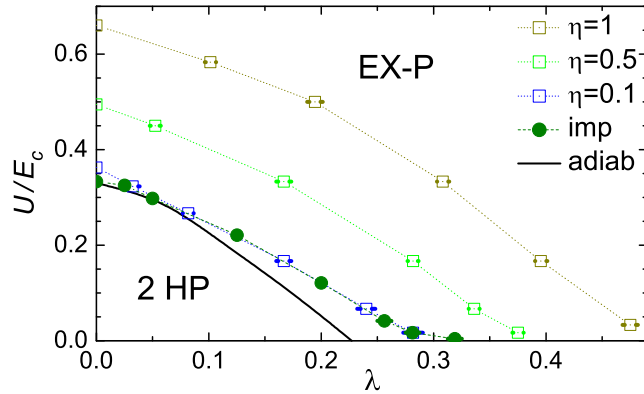


FIG. 6: (Color online) Phase diagram of the mass-asymmetric EX-P model with  $E_c = 3E_g$ ,  $E_v = \eta E_c$ , and  $\Omega = E_g$ . Solid line (solid circles) indicate transition line of the static impurity problem with  $\eta = 0$  [18] (obtained by exact numeric techniques [19, 20]). Dashed lines are guides to the eye.

interaction between E and H. In the antiadiabatic limit,  $\Omega \geq E_{c,v}$ , the retardation effects become negligible, and our model is equivalent to an effective attractive Hubbard model (EAHM) with  $U_{\text{eff}} = U + 2g^2/\Omega$  and hopping inverse proportional to the single HP mass  $t_{\text{eff}} = 1/m_{\text{HP}}$  (see, e.g., Ref. [11]). Comparing the EAHM data with results obtained for the full model where the retardation effects were included provides a good check for our DMC algorithm. Indeed we found good agreement for large phonon frequencies (see Fig. 5 for  $\Omega = 12E_g = 4E_c$ ). However, the domain of validity of the instantaneous approximation is rather limited. As seen from Fig. 5, the effective mass, e.g., considerably deviates from the exact result for  $\Omega \simeq E_c$  already.

To make contact with the situations for realistic semiconductors we construct the ground-state phase diagram for a set of mass asymmetries  $\eta = E_v/E_c < 1$  (Fig. 6). The data clearly show that the larger the bare mass of the hole  $m_h^0 \sim (E_v)^{-1}$ , the smaller  $U$  and  $\lambda$  are required to bind the excitonic QP. For  $\eta \rightarrow 0$  ( $m_h^0 \rightarrow \infty$ ) the hole

becomes almost immobile and the model is equivalent to that of a phonon-assisted localization on an attractive impurity [18]. The excellent agreement of our data with those obtained for the impurity problem by the Chebyshev space method [19] and DMC in direct space [20] provides one more successful test for the momentum space DMC technique (see Fig. 6). Surprisingly, the phase diagram of asymmetric EX-P binding well coincides with that of trapping by impurity already at  $\eta = 0.1$ .

In conclusion, we have developed an exact DMC algorithm for the interacting electron-hole-phonon system which fully takes into account an internal structure of the exciton-polaron. The technique is applicable to any band structure in  $D=1, 2$ , and  $3$ , an arbitrary (attractive) Coulomb interaction, and momentum-dependent fermion-phonon coupling. We constructed the phase diagram for a phonon-assisted electron-hole bound state formation, and discussed the change of the internal structure of an exciton-polaron in the transition regime. Comparison our exact results for the exciton-polaron problem with findings for an effective attractive Hubbard model shows that for realistic values of phonon frequencies the retardation effects can not be neglected.

We appreciate helpful discussions with A. Alvermann, F.X. Bronold, and M. Hohenadler. E.B. acknowledges financial support by DFG through SFB 652. A.S.M. is supported by RFBR 07-02-00067a.

- 
- [1] R. Knox, *Theory of excitons* (Academic Press, NY, 1963); A. Alexandrov (Ed.) *Polarons in Advanced Materials* (Springer-Verlag, Berlin 2007).
  - [2] I. Egri, Phys. Rep. **119**, 364 (1985).
  - [3] M. Ueta, H. Kanzaki, K. Kobayashi, Y. Toyozawa, and E. Hanamura, *Excitonic Processes in Solids*, (Springer-Verlag, Berlin 1986).
  - [4] H. Barentzen and V. Oudovenko, Europhys. Lett. **47**, 227 (1999).
  - [5] A. S. Mishchenko et al, Phys. Rev. B **66**, 020301 (2002).
  - [6] A. Sumi, J. Phys. Soc. Jpn. **43**, 1286 (1977).
  - [7] M. Hohenadler, P.B. Littlewood, and H. Fehske, Phys. Rev. B **76**, 184303 (2007).
  - [8] E. A. Burovski et al, Phys. Rev. Lett. **87**, 186402 (2001).
  - [9] S. Albrecht et al, Phys. Rev. Lett. **80**, 4510 (1998); L. X. Benedict, E. L. Shirley, and R. B. Bohn, *ibid* **80**, 4514 (1998); M. Rohlfing and S. G. Louie, *ibid* **81**, 2312 (1998).
  - [10] A. Marini, arXiv:0712.3365 .
  - [11] A. Macridin, G.A. Sawatzky, and M. Jarrell, Phys. Rev. B **69**, 245111 (2004).
  - [12] A.L. Fetter and J.D. Walecka, *Quantum Theory of Many-particle Systems* (New York: McGraw-Hill, 1971).
  - [13] N. Prokof'ev and B. Svistunov, Phys. Rev. Lett. **81**, 2514 (1998);
  - [14] A. S. Mishchenko et al, Phys. Rev. B **62**, 6317 (2000).
  - [15] The single polaron energy  $E_{\text{HP}}$  is calculated by the same computer by code setting  $U = 0$  and  $g_e(\mathbf{q}) = g_h(\mathbf{q}) \equiv g$ .
  - [16] J. P. Hague et al, Phys. Rev. B **73**, 054303 (2006).
  - [17] H. Kishida, N. Nagaosa, and Y. Tokura, Phys. Rev. B

- 53**, 12574 (1996).
- [18] Y. Shinozuka and Y. Toyozawa, J. Phys. Soc. Jpn. **46**, 505 (1979).
- [19] A. Alvermann and H. Fehske, Phys. Rev. B **77**, 045125 (2008).
- [20] A. S. Mishchenko et al, in preparation.